Solar Phys (2007) 241: 85–98
DOI 10.1007/s11207-006-0290-3

Acceleration Phase of Coronal Mass Ejections: I. Temporal and Spatial Scales

Bojan Vršnak · Darije Maričić · Andrew L. Stanger · Astrid M. Veronig · Manuela Temmer · Dragan Roša

Received: 11 August 2006 / Accepted: 13 November 2006 /
Published online: 27 February 2007

Abstract We study kinematics of 22 coronal mass ejections (CMEs) whose motion was traced from the gradual pre-acceleration phase up to the post-acceleration stage. The peak accelerations in the studied sample range from 40, up to 7000 $\mathrm{m\,s^{-2}}$, and are inversely proportional to the acceleration phase duration and the height range involved. Accelerations and velocities are, on average, larger in CMEs launched from a compact source region. The acceleration phase duration is proportional to the source region dimensions; *i.e.*, compact CMEs are accelerated more impulsively. Such behavior is interpreted as a consequence of stronger Lorentz force and shorter Alfvén time scales involved in compact CMEs (with stronger magnetic field and larger Alfvén speed being involved at lower heights). CMEs with larger accelerations and velocities are on average wider, whereas the widths are not related to the source region dimensions. Such behavior is explained in terms of the field

B. Vršnak (✉) · M. Temmer
Hvar Observatory, Faculty of Geodesy, Zagreb, Croatia
e-mail: bvrsnak@geodet.geof.hr

M. Temmer
e-mail: mat@igam.uni-graz.at

D. Maričić · D. Roša
Astronomical Observatory Zagreb, Opatička 22, 10000 Zagreb, Croatia

D. Maričić
e-mail: darije.maricic@zg.t-com.hr

D. Roša
e-mail: rosadragan@yahoo.com

A.L. Stanger
Royal Observatory of Belgium — SIDC, Brussels, Belgium
e-mail: Andrew.Stanger@oma.be

A.M. Veronig
IGAM/Institute of Physics, University of Graz, Graz, Austria
e-mail: asv@igam.uni-graz.at

pile-up ahead of the erupting structure, which is more effective in the case of a strongly accelerated structure.

Keywords Coronal mass ejections

1. Introduction

Coronal mass ejections (CMEs) show a broad variety of kinematic characteristics (*e.g.*, Yashiro *et al.*, 2004, and references therein). Most often, the eruption starts with a gradual evolution, characterized by a slow rise at an approximately constant velocity in the range $1-100\ \mathrm{km\,s^{-1}}$ (*e.g.*, Vršnak, 1998; Zhang and Dere, 2006, and references therein). This pre-acceleration phase may last for hours (Rompolt, 1990) and is usually considered to be an evolution through a series of equilibrium states. At a certain point, the rising structure starts to accelerate, which is attributed to the catastrophic loss of equilibrium (*e.g.*, Forbes, 2000; Lin, 2004, and references therein).

The CME take-off can be very impulsive — in extreme cases, the acceleration is so large that the CME achieves a velocity on the order of $1000\ \mathrm{km\,s^{-1}}$ below the height of, say, 0.2 solar radii (*e.g.*, Vršnak, 2001; Zhang *et al.*, 2001; Cliver *et al.*, 2004). In contrast, there are very gradual events, whose acceleration lasts for several hours, never exceeding $100\ \mathrm{m\,s^{-2}}$ (Zhang, 2005; Maričić, Vršnak, and Veronig, 2007a; Zhang and Dere, 2006).

The peak velocities range from several tens up to more than $2000\ \mathrm{km\,s^{-1}}$ (Gopalswamy, 2007). The fastest events are usually related to an impulsive acceleration, but not necessarily, since occasionally fast events show a gradual acceleration (Vršnak, Sudar, and Ruždjak, 2005). Apparently, the kinematic properties are related to the characteristics of the environment — impulsive events are usually launched from active regions, whereas the events launched from quiet regions are usually more gradual (Andrews and Howard, 2001). The most impulsive eruptions, attaining the highest velocities, are generally associated with powerful flares (*e.g.*, Gosling *et al.*, 1976; MacQueen and Fisher, 1983; for a discussion of the statistical aspect of the CME – flare relationship, see Vršnak, Sudar, and Ruždjak, 2005; Maričić *et al.*, 2007b).

In this paper, we analyze basic kinematic properties of a sample of twenty-two CMEs whose kinematics is fully covered by measurements from the pre-acceleration to the post-acceleration phase. We present a number of elemental relationships between the kinematical characteristics and the temporal/spatial scales involved in the eruption. The relationship between the CME acceleration phase and the energy release in the associated flare is analyzed in detail in the second paper of the series (Maričić *et al.*, 2007b).

2. Observations

2.1. Instruments

The basic sample of events consists of twenty eruptions recorded by the Mark-IV K-coronameter of the Mauna Loa Solar Observatory (MLSO). The Mark-IV coronagraph has the field of view from 1.1 to 2.8 solar radii and acquires white-light images with a cadence of 3 minutes.

The Mark-IV data are supplemented by the FeXII 195 Å images of the Extreme-ultraviolet Imaging Telescope (EIT) onboard the Solar and Heliospheric Observatory

(SOHO), which are used to trace the EUV coronal structures overlying the eruptive prominence in the early stage of the eruption. The EIT has a field of view of 1.4 solar radii (diagonal 1.9) and reveals coronal structures at temperatures around 1.6 MK (Delaboudiniere *et al.*, 1995).

At larger heights, CMEs were traced by employing the C2 and C3 white-light images of the Large Angle and Spectrometric Coronagraph (LASCO) onboard SOHO. Coronagraphs C2 and C3 cover the radial distance range 2.2 – 6 and 4 – 30 solar radii, respectively (Brueckner *et al.*, 1995).

The combined EIT, Mark-IV, and LASCO data enable a complete analysis of the CME kinematics, including the initiation, the acceleration phase, and the propagation phase. In this respect, the Mark-IV coronagraph provides the key measurements of the CME acceleration in the majority of analyzed events.

This basic set of twenty CMEs observed by the Mark-IV is supplemented by two CMEs of 17 January 2005, for which there are no Mark-IV data, but we had complete acceleration phase measurements from another study (Temmer *et al.*, 2007). In these two events, the acceleration phase was covered by the EIT/SOHO and the Solar X-ray Imager (SXI) onboard GOES (Hill *et al.*, 2005; Pizzo *et al.*, 2005). These two eruptions were included not only to enlarge the sample, but also because one of them was accelerated extremely impulsively, thus extending the range of the analyzed kinematical parameters.

2.2. Measurements

The propagation of CMEs, in all events considered, was traced by measuring the plane-of-sky heliocentric distance r of their leading edges (hereafter we express the distances also in units of the solar radius, $R = r/r_s$). In Figure 1 we show, as an example, the distance – time measurements for the event of 16 February 2003. The eruption was recorded in five EIT images, nine Mark-IV images, four LASCO-C2 images, and ten LASCO-C3 images.

Generally, the error of a single measurement varies from event to event, depending mainly on the contrast/sharpness of the leading edge. In most cases the radial distance of the leading edge can be estimated to an accuracy ranging from 0.02 – 0.05 solar radii in the case of EIT measurements and 0.05 – 0.1 solar radii in the case of Mark-IV, whereas in LASCO-C2 and LASCO-C3 it is usually in the range 0.1 – 0.3 and 0.3 – 1 solar radii, respectively. However, let us note that the main source of error might not be the inaccuracy of an individual measurement, but the uncertainty in identifying the same element of the eruption in successive images. In particular, this ambiguity becomes larger in cases where the measurements from different instruments do not overlap in time.

The method of deriving the velocity – and acceleration – time profiles is demonstrated in Figure 2. The procedure is based on the cubic-spline smoothing of the distance – time data in the interval covering the CME acceleration stage (for details see the Appendix, as well as Maričić *et al.*, 2004). From two successive smoothed data points, we evaluated the velocities:

$$v(t_{vi}) = \frac{r(t_{i+1}) - r(t_i)}{t_{i+1} - t_i}, \tag{1}$$

where $t_{vi} = (t_{i+1} + t_i)/2$. The accelerations are obtained from two successive velocity data points:

$$a(t_{ai}) = \frac{v(t_{vi+1}) - v(t_{vi})}{t_{vi+1} - t_{vi}}, \tag{2}$$

where $t_{ai} = (t_{vi+1} + t_{vi})/2$.

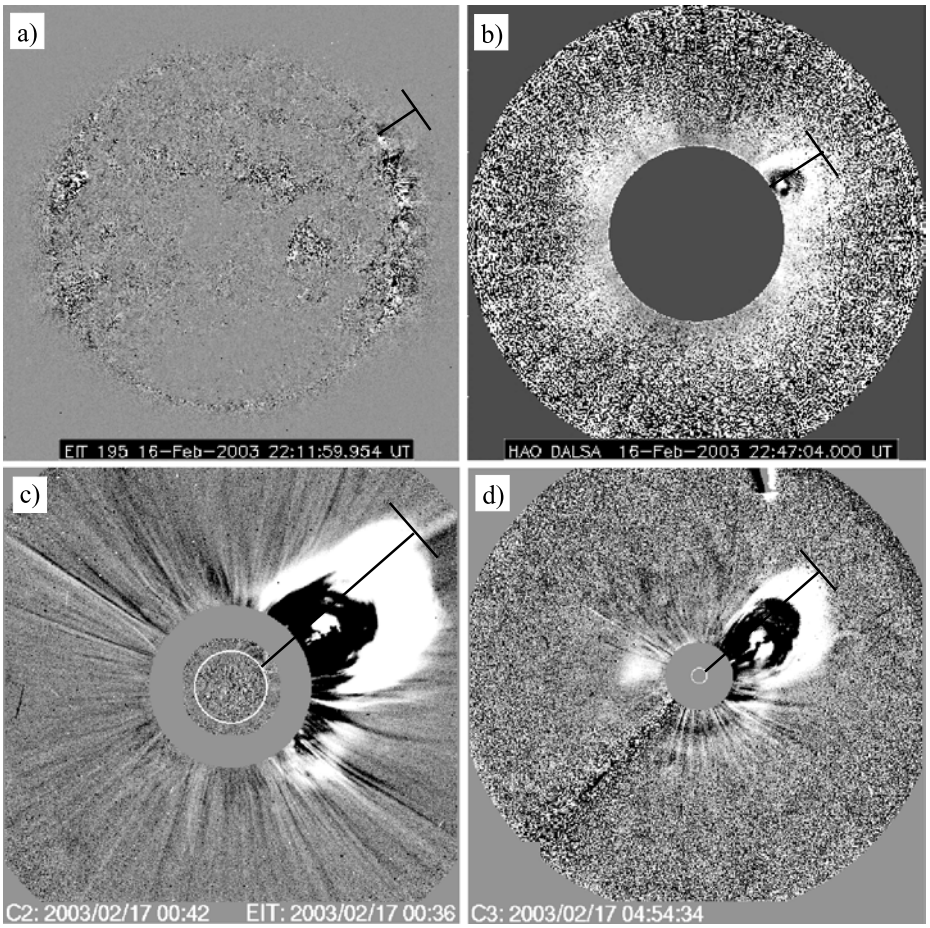

Figure 1 An example of the height – time measurements in running-difference images (the event of 16 February 2003; E9 in Table 1): (a) EIT Fe XII 195 Å; (b) Mark-IV; (c) LASCO-C2; (d) LASCO-C3. The Mark-IV field of view partly overlaps with the EIT and LASCO-C2 fields of view. In all images the T-shape marks the measured position of the leading edge.

From the acceleration – time profile we determined the times of the onset, the maximum, and the end of the acceleration phase (t_b, t_m, and t_e, respectively), as well as the peak acceleration ($a_{\max}$) and the duration of the acceleration phase ($T_{\rm acc} = t_e - t_b$). The average acceleration is obtained by applying

$$a_{\rm aver} = \frac{v_m - v_b}{t_{vm} - t_b}, \tag{3}$$

where v_m is the peak velocity, v_b is the velocity at the onset of the acceleration phase, and t_{vm} and t_b are the corresponding times. Note that in an ideal situation t_{vm} and t_e should be identical, but in real situations they usually have different values, since $a(t)$ often shows several "oscillations" around $a = 0$ at the end of the acceleration stage (see Figure 2d). Hence, the estimation of t_e is to a certain degree provisional. (For a discussion of the accuracy of the smoothing procedure see one more example shown in the Appendix.) In E9, presented

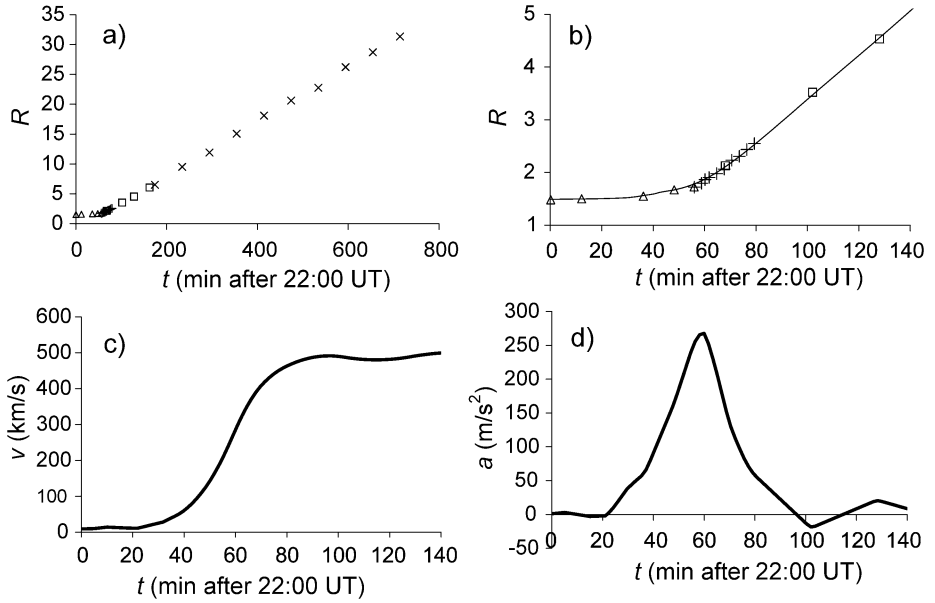

Figure 2 Kinematics of the CME of 16 February 2003 (E9 in Table 1). (a) Complete distance – time measurements (EIT Fe XII 195 Å — triangles, Mark-IV — pluses, LASCO-C2 — squares, and LASCO-C3 — crosses; the plane-of-sky heliospheric distance R is expressed in units of the solar radius); (b) the acceleration phase enlarged, shown together with the smoothed $R(t)$ curve; (c) the velocity – time profile $v(t)$, derived from the smoothed distance – time curve $R(t)$; (d) the acceleration – time profile $a(t)$ derived from the $v(t)$ curve. The size of symbols used in (b) depicts errors of measurements.

in Figure 2d, we estimated that the acceleration ended between $t = 95$ min (first $a = 0$) and $t = 115$ min (second $a = 0$), so we take for the end of the acceleration phase $t = 105$ min. Since the acceleration started around $t = 20$ min, we take for the acceleration phase duration $T_{\rm acc} = 85 \pm 10$ min. In most of the 22 analyzed events, the acceleration phase duration is estimated with a similar accuracy, generally ranging between 10% and 20%.

2.3. The Data Set

The analysis includes 22 events in which the basic CME structure was clearly recognizable already in the low corona, providing measurements of the CME kinematics from the initial up to late phases of the eruption. General characteristics of the chosen events are given in the first eight columns of Table 1, where the event label, the date, the location of the CME source region, its projected radial distance, the associated NOAA active region, the time of the CME first appearance in the LASCO-C2 field of view, the position angle PA of the measurement direction, and the CME angular width W (measured in the LASCO-C2/C3 field of view after it stabilizes at a constant value) are presented, respectively. Hereinafter, instead of using the dates, we use the event labels defined in the first column of Table 1.

Most of the events occurred close to the solar limb (see columns 3 and 4 of Table 1). The position of the CME source region was determined by measuring the coordinates of the midpoint between the footpoints of the erupting structure. In cases where footpoints could not be clearly identified, we used the coordinates of the centroid of the associated flare. The average projected radial distance of the source region is $\overline{R_0} = 0.9$ solar radii. In five events

Table 1 List of the analyzed CMEs and their characteristics. In the last two rows, the average values and standard deviations are given.

Label	Date	Location	$R_0 = \frac{r_0}{r_s}$	NOAA	t_{C2} UT	PA deg	W deg	v_m km s^{-1}	T_{acc} min	a_{max} m s^{-2}	a_{aver} m s^{-2}
E1	26-Feb-00	N29E50	0.83	8889	23:54	4	104	1110	97	234	146
E2	28-Jun-00	N20W90	1	9046	19:31	290	>134	1466	48	1293	484
E3	23-Apr-01	S28W90	1	–	19:09	230	80	365	340	40	20
E4	15-May-01	N15E90	1	9461	18:52	45	195	1224	140	404	150
E5	25-May-01	S12E90	1	–	17:26	120	208	958	122	300	170
E6	8-Jan-02	N53W27	0.84	9773	18:30	345	68	480	144	120	57
E7	9-Mar-02	S10E66	0.92	9866	22:30	75	64	370	48	270	128
E8	6-Jun-02	N34E90	1	9986	17:54	25	69	745	240	90	54
E9	16-Feb-03	N20W90	1	10278	23:08	305	151	491	85	270	107
E10	18-Feb-03	N65W75	0.99	–	02:42	310	93	802	155	209	87
E11	14-Mar-03	S20W66	0.92	10304	18:06	210	137	881	57	382	151
E12	15-Mar-03	N07E67	0.92	–	21:54	15	125	629	295	76	38
E13	26-Apr-03	N16E47	0.75	10346	21:50	20	166	705	152	193	89
E14	12-Jul-03	N16E76	0.97	10409	19:31	75	58	412	23	335	220
E15	15-Jul-03	N29W90	1	–	22:30	305	59	540	107	132	46
E16	21-Oct-03	S18E87	1	10486	19:54	100	47	640	412	51	29
E17	22-Oct-03	S17E88	1	10486	20:06	94	134	1143	12	3975	1543
E18	26-Oct-03	N04W43	0.68	10484	17:54	280	>171	1366	50	1166	360
E19	12-Nov-03	S05W80	0.98	10498	18:30	260	88	940	61	363	241
E20	18-Aug-04	S12W88	1	10656	17:54	250	120	740	40	766	389
E21	17-Jan-05A	N14W23	0.45	10720	09:30	280	360	2084	127	423	257
E22	17-Jan-05B	N14W23	0.45	10720	09:54	280	360	2775	13	7316	3434
average			0.9				>136	948	126	836	373
stdev			0.17				86	560	108	1670	92

(E4, E5, E8, E9, and E15), the footpoints of the erupting structure were partly behind the limb.

The CMEs widths were in the range $W \approx 60° - 360°$ (column 8 of Table 1 and Figure 3a), with a mean value of $W_{aver} = 136°$; *i.e.*, the CMEs from our sample are wider than average (*e.g.*, Yashiro *et al.*, 2004, found $\overline{W} \approx 50° - 60°$). Five eruptions showed a very prominent three-part structure (frontal rim, cavity, and bright core). On average, the angular widths of CMEs decrease toward the limb with the $W(R_0)$ relationship characterized by a correlation coefficient $C = 0.51$ and an F-test statistical significance $P \approx 98\%$. (The significance $P > 98\%$ implies that the probability of no correlation between two parameters is less than 2%.)

3. Results

In columns 9 – 12 of Table 1, we present the basic kinematic properties of the CMEs:

- the highest speed v_m found from the smoothed velocity – time profile;
- the acceleration phase duration ($T_{acc} = t_e - t_b$);
- the peak acceleration a_{max}; and
- the mean acceleration a_{aver} (Equation (3)).

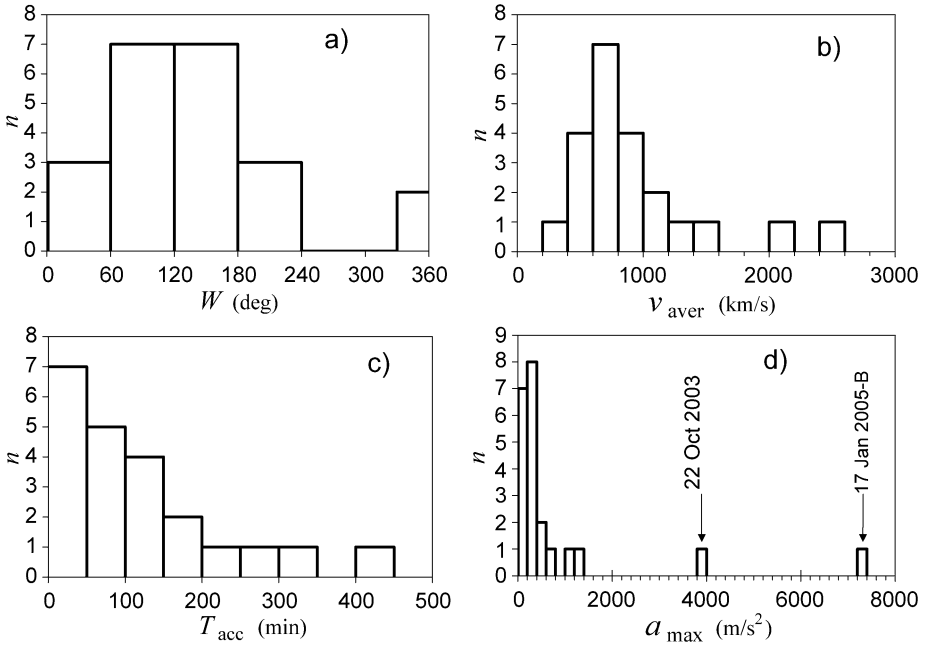

Figure 3 Distribution of (a) CME widths; (b) average velocities; (c) acceleration phase durations (with a shortest observed acceleration phase of 12 min); and (d) peak accelerations.

In Figure 3b, we show the distribution of the CME mean velocities in the LASCO-C2/C3 field of view. The distribution peaks at the bin 600 – 800 km s^{-1} (with an average value of 940 km s^{-1}), which is considerably faster than in an average CME sample (*e.g.*, Yashiro *et al.*, 2004 found $\overline{v} \approx 300 - 500$ km s^{-1}). A very similar result occurs if the mean velocities are replaced by the peak velocities that are shown in column 9 of Table 1.

On average, the events with a source region closer to the disc center were faster than those located close to the limb, *i.e.*, opposite from what one would expect, bearing in mind the projection effects. The relationship is characterized by a correlation coefficient $C = 0.52$ and an F-test statistical significance $P \approx 98\%$. No statistically significant correlation was found between the CME acceleration and the source region position.

The distribution of the acceleration phase durations and the peak accelerations are presented in Figures 3c and 3d, respectively. The acceleration phase durations, $T_{\rm acc}$, range from 12 min up to almost 7 hours, with a mean value of 120 min (Table 1). The peak accelerations, $a_{\rm max}$, vary from 40 up to 7300 m s^{-2} (with a mean value of 840 m s^{-2}). As expected, the peak accelerations are roughly twice as large as the mean accelerations $a_{\rm aver}$ (compare columns 11 and 12 in Table 1).

Inspecting Table 1, we find that larger accelerations are associated with shorter acceleration phase durations. The dependencies of the peak and mean accelerations on the acceleration phase duration are shown in Figure 4a. The graph shows distinct anti-correlations, where the two power-law fits have almost identical slopes ($b = -1.08 \pm 0.14$ and $b = -1.10 \pm 0.14$). Such a relationship is quite similar to that found by Zhang (2005) and Zhang and Dere (2006), who analyzed a sample of CMEs recorded by LASCO-C1. The power-law dependencies for the average acceleration reported therein are characterized by similar slopes, $b = -1$ and $b = -1.09$, respectively, but are shifted by a factor of 1.7 and 1.4 to

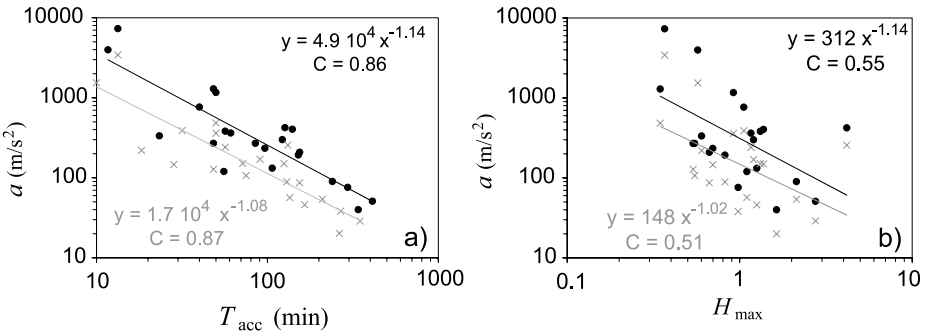

Figure 4 Peak accelerations (black dots) and mean accelerations (gray crosses), shown as a function of (a) the acceleration phase duration and (b) the height at which the peak acceleration was attained. The F-test statistical significance of the correlations in (a) is $P > 99\%$, whereas in (c), it is $P > 98\%$. Note that the errors of individual values of the acceleration are smaller than the scatter of data points.

lower values. However, if we exclude from our sample the very strongly accelerated E22, we come to an almost perfect match with the result of Zhang (2005) and Zhang and Dere (2006).

In Figure 4b, we show the peak and mean accelerations as a function of the plane-of-sky height $H_{\max}$ at which the peak acceleration was attained (where $H_{\max}$ is expressed in units of the solar radius). The graph shows that events which were accelerated at lower heights achieved stronger accelerations. Note that if the event of the largest $H_{\max}$ would be removed (E21), the correlation coefficient would increase from $C = 0.55$ (see the inset in Figure 4b) to $C = 0.68$. The dependence shown in Figure 4b is similar to that presented by Vršnak (2001). Accelerations displayed therein show a decrease from several 1000 $\mathrm{m\,s^{-2}}$ close to the surface to $a_{\max} \approx 10-20\ \mathrm{m\,s^{-2}}$ at $H_{\max} \approx 10$, which is quite similar to the dependence presented in Figure 4b.

A relationship very similar to that shown in Figure 4b is found if $H_{\max}$ is replaced by the height at which the acceleration ended ($a_{\max} \approx 1000 \times H_{\mathrm{end}}^{-0.86}$; not shown). Such a relationship demonstrates that ejections accelerated over a longer distance range are characterized by weaker acceleration.

In Figures 5a and 5b, we show the correlation between the CME angular width W and the CME acceleration and velocity. The graphs show a distinct correlation between the kinematical (a, v) and geometrical (W) properties of CMEs. The faster and more strongly accelerated CMEs tend to be wider. (For the $W(v)$ relationship in much larger samples see Hundhausen, Burkepile, and St. Cyr, 1994, Yashiro *et al.*, 2004, and Vršnak, Sudar, and Ruždjak, 2005.)

Such an outcome is a bit surprising from the theoretical point of view (to be discussed in Section 4), since it is expected that, initially, compact CMEs (with small dimensions) should show a stronger and a more impulsive acceleration than the extended CMEs (Vršnak, 2006). So, we performed an alternative analysis, in which we inferred the overall dimensions of the CME source region, by measuring the length of the eruptive filament, the extent of the coronal dimming, and the distance to remote (stationary) brightenings. (For different possibilities of determining dimensions of CME source regions see Cremades and Bothmer, 2004 and Chen *et al.*, 2006.)

In Figures 5c and 5d, we show the dependence of the mean acceleration and the acceleration phase duration on the inferred dimension of the CME source region, d. As mentioned in Section 2.3, in five events the footpoints of CMEs were partly behind the limb, so we could

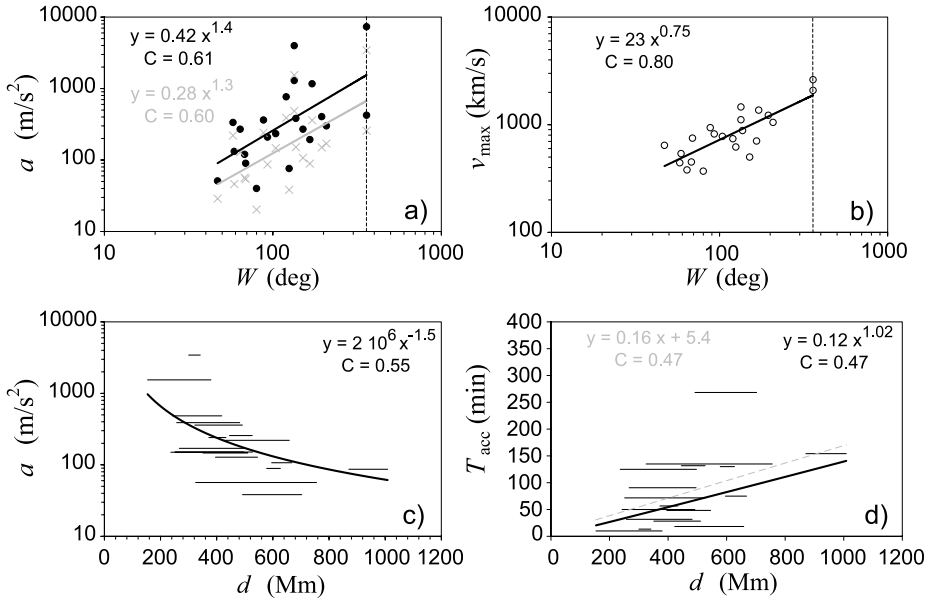

Figure 5 Relationship between (a) the CME acceleration a and the CME width W (black — peak accelerations, gray — mean accelerations); (b) the CME peak velocity and the CME angular width; (c) the acceleration and the source region dimension d (horizontal bars represent the uncertainty range); and (d) the acceleration phase duration, $T_{\rm acc}$, and the source region dimensions. Insets show the least-squares fits. Vertical dashed lines in (a) and (b) mark $W = 360^{\circ}$ halo CMEs. All correlations shown in (a) – (d) have F-test statistical significance $P > 99\%$.

estimate d only in 17 events. We emphasize that measurements of d are quite difficult to make and subject to personal judgment, so we used a span of values from the smallest to the largest reasonable values (horizontal bars in Figures 5c and 5d). Generally, the lower limit of d was determined from the separation of the erupting filament footpoints. In the events where the footpoints could not be identified unambiguously, we used the extent of flare brightenings along the magnetic inversion line. The upper limit was determined by measuring the largest distance between disturbed coronal structures adjacent to the CME-associated magnetic neutral line or stationary patterns of coronal dimming.

The presented graphs show a distinct anti-correlation between a and d, and a proportionality between $T_{\rm acc}$ and d. If only upper limits on d are taken into account, the correlation coefficient becomes $R = 0.81$, whereas for lower limits it is $R = 0.57$. We found also an anti-correlation between v and d (not shown), similar to that of a and d, though of a somewhat lower statistical significance ($P \approx 97\%$). No correlation is found between CME widths W and the source region dimension d, nor between W and the duration of the acceleration phase, $T_{\rm acc}$.

4. Discussion and Conclusions

We summarize the results of our analysis as follows:

1. The CME acceleration is inversely proportional to the acceleration phase duration (Figure 4a) and the height range involved (Figure 4b).

2. The highest observed acceleration peak was larger than 7000 m s^{-2} (Figure 3d).
3. Accelerations (and velocities) are on average larger in CMEs launched from a compact source region (Figure 5c).
4. The acceleration phase duration is proportional to the source region dimensions; *i.e.*, compact CMEs are accelerated more impulsively (Figure 5d).
5. CMEs of larger acceleration and velocity are on average wider (Figures 5a and 5b).
6. The CME widths are not related to the source region dimensions.

Inspecting Table 1, one finds that the accelerations and acceleration phase durations are scattered over a wide range of values. In our sample, the strongest acceleration is roughly 170 times larger than the weakest acceleration, and the ratio of shortest-to-longest acceleration phase duration is 1:35. However, because of the $a \propto T^{-1}$ relationship (summary item 1), the scatter of velocities is not that large. The lowest and the highest peak velocities are 365 and 2775 km s^{-1}, which gives a ratio of 1:7.

Such a behavior probably reflects the fact that CMEs are driven by the Lorentz force. In that case, the kinetic energy density cannot exceed the magnetic energy density; *i.e.*, $\rho v^2/2 \leq B^2/2\mu_0$, or rewritten, $v^2 \leq B^2/\rho\mu_0$. In other words, the CME velocity cannot be larger than the Alfvén velocity within the pre-eruptive structure ($v \leq v_A$). The scatter of CME velocities indicates that values of the Alfvén velocity in the pre-eruptive coronal structures are confined to within an order of magnitude. That is consistent with some other measurements in the height range of one solar radius above the solar surface (see Vršnak *et al.*, 2002, and references therein). At these heights, the inferred values of the Alfvén velocity are found in the range 300 – 1500 km s^{-1}, corresponding to a ratio of 1:5.

An order of magnitude estimate of the CME acceleration can be written as $a = v/t \leq v_A/t_A = v_A/(d/v_A) = v_A^2/d$, where $t_A = d/v_A$ represents the Alfvén travel time across the erupting structure. Another way to get this expression is to consider the magnetic stress, which can be expressed approximately as $a \leq B^2/2\mu_0 d$, again giving $a \leq v_A^2/d$. Taking $v_A = 1000$ km s^{-1} and $d = 100$ Mm, one finds $a \leq 10^4$ m s^{-2}, which illustrates that accelerations exceeding 1000 m s^{-2} should not be surprising in compact CMEs (*e.g.*, $d \approx 100$ Mm). However, the accelerations such as that in E22 (summary item 2), or in the event of 6 November 1997 described by Zhang *et al.* (2001) and Cliver *et al.* (2004), are probably close to the upper limit.

The relationship $a \leq v_A^2/d$ also implies that eruptions of compact structures (small d) on average should have accelerations larger than extended eruptions, which is consistent with our measurements (summary item 3). Taking also into account $a = v/t$, one finds $T_{\rm acc} \geq d/v_A$; *i.e.*, compact CMEs should be accelerated more impulsively, consistent with our results (summary items 1 and 4). Furthermore, the co-existence of the relationships $a \propto d^{-1}$ (or $a \propto H_{\rm max}^{-1}$ shown in Figure 4b) and $v \propto d$ explains straightforwardly the inverse proportionality of a and $T_{\rm acc}$ shown in Figure 4a.

In this respect, it is worth noting that the analytical models by Vršnak (1990) and Chen and Krall (2003), which treat CMEs as toroidal field structures, predict that accelerations should be larger in the case of smaller footpoint separation. Moreover, these models predict that the peak acceleration should be attained close to or after the height becomes comparable with the footpoint half-separation. Evidence for such a scaling was found by Chen *et al.* (2006). Although our results are consistent with such a scaling (acceleration is inversely proportional to both d and $H_{\rm max}$), a direct comparison of $H_{\rm max}$ and d does not show a statistically significant correlation $H_{\rm max}(d)$. For the ratio $H_{\rm max}/d$ we find a broad range of values, spanning from 0.5 to 5. However, it should be noted that our sample is rather small and that measurements of d and $H_{\rm max}$ are burdened with large errors. Finally, we note

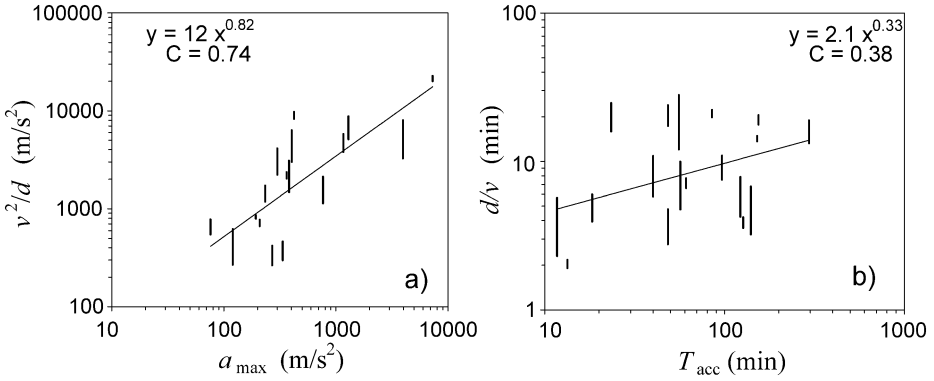

Figure 6 (a) The values of the parameter v^2/d, shown as a function of the observed peak accelerations. (b) The values of the parameter d/v shown as a function of the observed acceleration phase durations. The least-squares fit parameters are given in the insets; the F-test significance is $P > 99\%$ and $P > 97\%$, respectively.

that the model by Kliem and Török (2006) is also consistent with our result that compact events show higher accelerations. In this current-ring model, where the eruption is driven by the torus instability, such a scaling is a consequence of the behavior of the overlying field. However, it should be noted that the model is still incomplete, since it does not yet include a realistic description of the line-tying.

In Figures 6a and 6b, we compare the parameters v^2/d and d/v with $a_{\max}$ and $T_{\rm acc}$, respectively. Both graphs show a distinct correlation ($P > 99\%$ and $P > 97\%$, respectively). The former relationship has two aspects: a kinematic one (generally $a \propto v^2/h$, where h is the height) and a dynamic one ($v_m \propto v_A$ and $a_{\max} \propto 1/d$). Bearing in mind both aspects, we should consider the parameter v^2/d as an upper limit to the possible accelerations at a given d and, analogously, the parameter d/v as a lower limit for $T_{\rm acc}$. Indeed, Figure 6 shows that the observed accelerations a are lower by a factor of several than the expected upper limit accelerations v^2/d, whereas the acceleration phase durations are several times longer than the expected lower limit durations d/v.

The correlations $a(W)$ and $v(W)$ shown in Figures 5a and 5b (summary item 5) apparently contradict previous interpretation, if the CME width is considered as a measure of the size of the erupting structure. The only way around the problem is to re-interpret the $a - W$ and $v - W$ relationships, by saying that strongly accelerated fast eruptions cause wide CMEs, and that the CME width is not directly related to the initial size of the erupting structure. Indeed, the latter assumption is consistent with our summary item 6. (For a discussion see Figure 7 of Cremades and Bothmer, 2004, showing that CMEs of small source region dimensions may be as wide as those originating from very extended sources.) This is supported also by the fact that very fast CMEs, associated with the most powerful flares, are usually launched from a compact source within an active region, and still most of them become halo or partial-halo CMEs. In this respect, the source region location and the related projection effects also play an important role.

The acceleration – width and the velocity – width relationships may be understood in terms of the snow-plough effect (*e.g.*, Tappin, 2006). When an eruption is strongly accelerated, the magnetoplasma overlying the erupting structure has no time to slide down aside the CME flanks, but accumulates at the CME front. The increase of the accumulated overlying magnetic flux implies that field lines of successively larger turnover height become dragged

by the eruption. Since loops of a higher turnover are also wider, the angular width of impulsively accelerated CMEs is, on average, larger than that of gradually accelerated CMEs. The described snow-plough scenario is consistent with the increase of the CME width during the take-off phase and the expanding coronal dimming (Chen *et al.*, 2005).

Acknowledgements This work is sponsored by the Air Force Office of Scientific Research, USAF, under Grant No. FA8655-06-1-3036. M.T. and A.V. acknowledge the support by the Austrian Science Fund (FWF Grant Nos. P15344 and J2512-N02). We are grateful to the GOES, MLSO, and SOHO teams for developing and operating the instruments and we appreciate their open data policies. We are thankful to Dr. Tibor Török (the referee) and Drs. Edward W. Cliver, Nariaki Nitta, and Werner M. Neupert for constructive comments and suggestions that led to a significant improvement of the paper.

Appendix: The Smoothing

In the presented analysis we utilized the cubic-spline smoothing of the distance – time data. The shapes of the smoothed curves, and thus the derived velocities and accelerations, depend on the spline degree (hereinafter denoted as N) and the interval chosen for smoothing. Most generally speaking, when a smaller spline degree is applied, the resulting curves are smoother and the deviations of the smoothed curve from the data points are larger. Consequently, the acceleration curve derived from the smoothed $R(t)$ data has an underestimated amplitude if the spline degree is too low. However, a too high spline degree does not smooth the raw data significantly, leaving a too noisy acceleration – time profile. The choice of the smoothing interval affects the distribution of knots in the spline smooth algorithm and thus

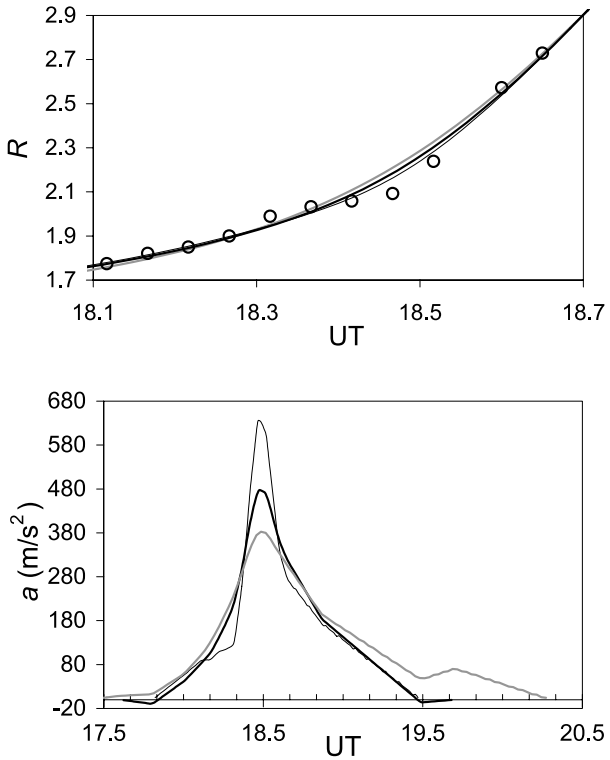

Figure 7 Smoothing of the $R(t)$ data for E4: raw data $R_i(t_i)$ with smoothed curves $R(t)$ (top) and acceleration curves (bottom), obtained by spline degree $N = 6$ at smoothing intervals 17:48 – 19:29 UT (thin), 17:36 – 19:42 UT (bold), and 17:24 – 20:18 UT (gray). Minor ticks on the x-axes represent 10-min intervals.

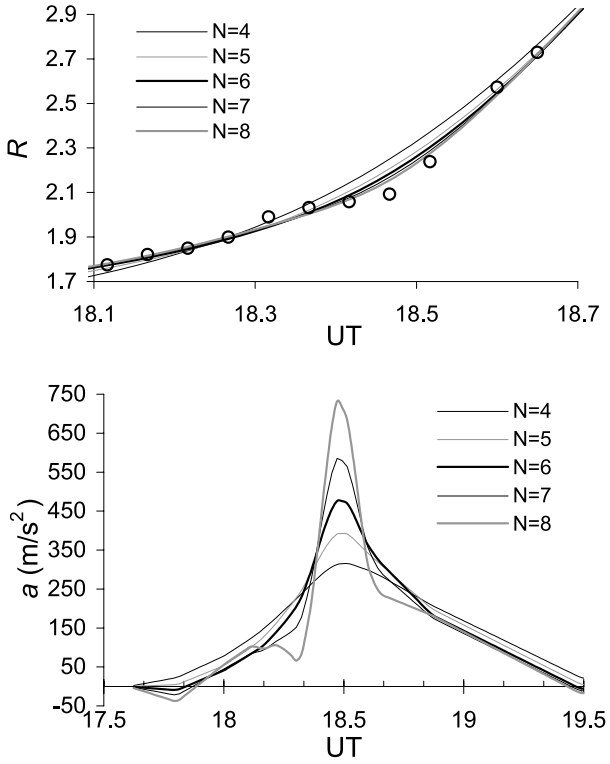

Figure 8 Smoothing with various spline degrees for the interval 17:36 – 19:42 UT. Raw data $R_i(t_i)$ and smoothed curves $R(t)$ are shown in the top panel; the corresponding acceleration curves $a(t)$ are shown in the bottom panel. Thin-black, thin-gray (dashed), bold-black, thin-black (dashed), and bold-gray lines represent the outcome for spline degree $N = 4$, 5, 6, 7, 8, respectively (successively from lowest to largest acceleration peak values).

indirectly influences the shape of the smoothed curve. In the following we illustrate these two effects, primarily to depict the accuracy of the estimated acceleration amplitudes, onset times, and peak times. For this purpose we employ the event E4, which occurred on 15 May 2001 (see also Maričić *et al.*, 2004).

In Figure 7 we illustrate the way in which the variations of the smoothing interval affect the acceleration curve. Figure 7 shows that the acceleration peak time does not depend significantly on the choice of the smoothing interval. Similarly, the onset pattern is not much affected. However, a significant difference appears in the acceleration decay phase, mainly because the data points are widely separated in that stage.

In Figure 8 we compare curves obtained by applying different spline degrees. The upper panel shows that the smoothings with lowest spline degrees ($N \leq 5$) results in significant deviations from the raw data, and thus these are not appropriate to describe the CME acceleration. The other, higher spline degree options ($N \geq 6$) reproduce the raw data much better. They all show a similar acceleration timing, but the amplitude differs significantly. Note that the curve obtained by applying $N = 8$ reveals a precursor-like bump in the acceleration curve, which in fact can be seen also directly in the top panels of Figures 7 and 8 as the bump in the leading-edge raw data, starting around 18:15 UT. The smoothing with $N > 8$ already results in a very noisy acceleration showing several episodes of $a < 0$. So, we suppose that $6 \leq N \leq 8$ represents the range of spline degrees appropriate to smooth the $R(t)$ data in the considered event. Inspecting the acceleration curves in the bottom panel of Figure 8, one finds 600 ± 150 m s^{-2}. In most of the 22 analyzed events, the smoothing procedure provides a similar level of accuracy.

References

Andrews, M.D., Howard, R.A.: 2001, *Space Sci. Rev.* **95**, 147.
Brueckner, G.E., Howard, R.A., Koomen, M.J., *et al.*: 1995, *Solar Phys.* **162**, 357.
Chen, J., Krall, J.: 2003, *J. Geophys. Res.* **108**, 1410.
Chen, J., Marqué, C., Vourlidas, A., Krall, J., Schuck, P.W.: 2006, *Astrophys. J.* **649**, 452.
Chen, P.F., Fang, C., Shibata, K.: 2005, *Astrophys. J.* **622**, 1202.
Cliver, E.W., Nitta, N.V., Thompson, B.J., Zhang, J.: 2004, *Solar Phys.* **225**, 105.
Cremades, H., Bothmer, V.: 2004, *Astron. Astrophys.* **422**, 307.
Delaboudinière, J.-P., Artzner, G. E., Brunaud, J., *et al.*: 1995, *Solar Phys.* **162**, 291.
Forbes, T.G.: 2000, *J. Geophys. Res.* **105**, 23153.
Gopalswamy, N.: 2007, *Sun Geosph.*, in press.
Gosling, J.T., Hildner, E., MacQueen, R.M., Munro, R.H., Poland, A.I., Ross, C.L.: 1976, *Solar Phys.* **48**, 389.
Hill, S.M., Pizzo, V.J., Balch, C.C., *et al.*: 2005, *Solar Phys.* **226**, 255.
Hundhausen, A.J., Burkepile, J.T., St. Cyr, O.C.: 1994, *J. Geophys. Res.* **99**, 6543.
Kliem, B., Török, T.: 2006, *Phys. Rev. Lett.* **96**, 255002.
Lin, J.: 2004, *Solar Phys.* **219**, 169.
MacQueen, R.M., Fisher, R.R.: 1983, *Solar Phys.* **89**, 89.
Maričić, D., Vršnak, B., Stanger, A.L., Veronig, A.: 2004, *Solar Phys.* **225**, 337.
Maričić, D., Vršnak, B., Veronig, A.: 2007a, In: Chillingarian, A., Karapetyan, G. (eds.) *Proceedings of the Second International Symposium: Solar Extreme Events*, p. 41.
Maričić, D., Vršnak, B., Stanger, A.L., Veronig, A., Temmer, M., Roša, D.: 2007b, *Solar Phys.*, this issue, doi:10.1007/s11207-007-0291-x.
Pizzo, V.J., Hill, S.M., Balch, C.C., *et al.*: 2005, *Solar Phys.* **226**, 283.
Rompolt, B.: 1990, *Hvar Obs. Bull.* **14**, 37.
Tappin, S.J.: 2006, *Solar Phys.* **233**, 233.
Temmer, M., Vršnak, B., Veronig, A., Miklenic, C.: 2007, *Cent. Eur. Astrophys. Bull.* **31**, in press.
Vršnak, B.: 1990, *Solar Phys.* **129**, 295.
Vršnak, B.: 1998, *ASP Conf. Ser.* **150**, 302.
Vršnak, B.: 2001, *J. Geophys. Res.* **106**, 25249.
Vršnak, B.: 2006, *Adv. Space Res.* **38**, 431.
Vršnak, B., Magdalenić, J., Aurass, H., Mann, G.: 2002, *Astron. Astrophys.* **396**, 673.
Vršnak, B., Sudar, D., Ruždjak, D.: 2005, *Astron. Astrophys.* **435**, 1149.
Yashiro, S., Gopalswamy, N., Michalek, G., *et al.*: 2004, *J. Geophys. Res.* **109**, A07105.
Zhang, J.: 2005, In: Dere, K., Wang, J., Yan, Y. (eds.) *Coronal and Stellar Mass Ejections*, IAU Symp., vol. **226**, p. 65.
Zhang, J., Dere, K.P.: 2006, *Astrophys. J.* **649**, 1100.
Zhang, J., Dere, K.P., Howard, R.A., Kundu, M.R., White, S.M.: 2001, *Astrophys. J.* **559**, 452.